Check for updates

Self-assembly of a silicon-containing side-chain liquid crystalline block copolymer in bulk and in thin films: kinetic pathway of a cylinder to sphere transition†

Fen Liao, [ID] [a] Ling-Ying Shi, [ID] *[a,b] Li-Chen Cheng, [ID] [b] Sangho Lee, [ID] [b] Rong Ran, [ID] [a] Kevin G. Yager [ID] [c] and Caroline A. Ross [ID] *[b]

The self-assembly of a high-χ silicon-containing side-chain liquid crystalline block copolymer (LC BCP) in bulk and in thin films is reported, and the structural transition process from the hexagonally packed cylinder (HEX) to the body-centered cubic structure (BCC) in thin films was examined by both reciprocal and real space experimental methods. The block copolymer, poly(dimethylsiloxane-*b*-11-(4′-cyanobiphenyl-4-yloxy)undecylmethacrylate) (PDMS-*b*-P(4CNB11C)MA) with a molecular weight of 19.5 kg mol^{-1} and a volume fraction of PDMS 27% self-assembled in bulk into a hierarchical nanostructure of sub-20 nm HEX cylinders of PDMS with the P(4CNB11C)MA block exhibiting a smectic LC phase with a 1.61 nm period. The structure remained HEX as the P(4CNB11C)MA block transformed to an isotropic phase at ~120 °C. In the thin films, the PDMS cylindrical microdomains were oriented in layers parallel to the substrate surface. The LC block formed a smectic LC phase which transformed to an isotropic phase at ~120 °C, and the microphase-separated nanostructure transformed from HEX to BCC spheres at ~160 °C. The hierarchical structure as well as the dynamic structural transition of the thin films were characterized using *in situ* grazing-incidence small-angle X-ray scattering and grazing-incidence wide-angle X-ray scattering. The transient morphologies from the HEX to BCC structure in thin films were captured by scanning electron microscopy and atomic force microscopy, and the transition pathway was described.

Introduction

The self-assembly of block copolymers (BCPs) has been intensively investigated because of their ability to provide a variety of well-defined nanostructures with length scales of a few nm to over 100 nm, with applications in many nanotechnologies.[1–8] The introduction of a liquid crystalline

[a]College of Polymer Science and Engineering, State Key Laboratory of Polymer Materials Engineering, Sichuan University, Chengdu 610065, China.
E-mail: shilingying@scu.edu.cn
[b]Department of Materials Science and Engineering, Massachusetts Institute of Technology, 77 Massachusetts Avenue, Cambridge, Massachusetts 02139, USA.
E-mail: caross@mit.edu
[c]Center for Functional Nanomaterials, Brookhaven National Laboratory, Upton, NY, 11973, USA

†Electronic supplementary information (ESI) available: Schematic illustration of the chain conformations of the block copolymer in different temperature ranges; cross-section SEM images of the PDMS-*b*-P(4CNB11C)MA BCP thin film; calculation of the length of the cyanobiphenyl LC group; top view SEM image of the drop-cast thick thin film and of the thin film without thermal annealing; and schematic illustration of the $\chi_{eff}N$ value location in the phase diagram at different temperatures. See DOI: 10.1039/c8nr07685e

polymer into BCPs produces the so-called liquid crystalline block copolymers (LCBCPs) which can form various hierarchical nanostructures with advanced functionalities.[9–13] The LCBCPs not only enrich the possible microphase-separated morphologies but also enhance morphological control *via* the complex interplay between microphase separation and LC ordering.[14–17] As an example, the orientation and phase transition of the liquid crystalline blocks of the LCBCPs induce changes in the microdomain geometry, which results in abundant opportunities for order-to-order structural transitions.[18–20] Moreover, compared with conventional coil–coil BCPs, the LCBCPs may exhibit a stronger driving force for phase separation under the influence of the LC ordering,[21,22] which makes LCBCPs excellent candidates for obtaining useful nanostructures.

For applications such as nanolithography where small feature sizes are required, high interaction parameter (χ) block copolymers are preferred.[23] Among various high-χ block copolymers that have been studied, silicon-containing block copolymers including polyhedral oligomeric silsesquioxane- (POSS-), polyferrocenylsilane- (PFS-), and polydimethylsiloxane (PDMS) blocks are attractive due to the high etch contrast for robust

pattern transfer.[24–27,28,29] If a silicon-containing block is combined with an organic LC block, the resulting high-χ silicon-containing LCBCPs are expected to produce hierarchical nanostructures with small-scale periodicities and with etch contrast for pattern transfer. Thus, silicon containing LCBCPs may open fascinating possibilities for the preparation of nanomaterials.

In order to generate thin film nanotemplates and scaffolds from block copolymers, the morphology as well as ordering and orientation control of microdomains in the BCP films is crucial.[30–32] The LCBCPs, *e.g.* with cyanobiphenyl- and azobenzene-side chains, are responsive to magnetic, light and electric fields as well as thermal and mechanical forces, facilitating control over the ordering and orientation of the microdomains.[33–37] For example, the application of external fields such as photoalignment or magnetic and electric fields to control the LC orientation of side chain LCBCPs can induce uniform macroscopic orientation of the microdomains.[15,18–20,38,39] Furthermore, although extensive studies of the equilibrium morphologies in the thin films of various block copolymers have been widely reported, the structural evolution processes of the BCP thin films are still poorly understood. Knowledge of the ordering pathways and transition process is a prerequisite both for eliminating kinetically-trapped defects in BCP thin films[40–43] and for understanding how LC phase transitions could induce order–order transitions.[44–46]

Here, we present the self-assembly behavior in bulk and in thin films of a silicon-containing side-chain liquid crystalline block copolymer poly(dimethylsiloxane-*b*-11-(4′-cyanobiphenyl-4-yloxy)undecylmethacrylate) or PDMS-*b*-P(4CNB11C)MA, where the molecular weights M_n of PDMS and P(4CNB11C)MA are 5.0 and 14.5 kg mol^{-1}, respectively (Fig. 1a). The bulk phase behavior was investigated by small-angle X-ray scattering (SAXS) and transmission electron microscopy (TEM), showing that a hexagonal closepacked structure with sub-20 nm periodicity formed within a wide temperature range. For 140 nm thick films the hierarchical nanostructure and the relative orientation between the smectic LC ordering and the microdomains and the structural transitions were investigated using grazing-incidence small-angle X-ray scattering (GISAXS) and wide-angle X-ray scattering (GIWAXS) measurements. In addition, the cylindrical to spherical structural transition and the transient morphology were observed by SEM and AFM methods. The results of this study of the thin film behavior of the high-χ PDMS-*b*-P(4CNB11C)MA LC block copolymer will enable applications of this material to nanofabrication and nanotechnology.

Experimental

The PDMS-*b*-P(4CNB11C)MA block copolymer was purchased from Polymer Source Inc. The molecular weights of PDMS and P(4CNB11C)MA were 5.0 and 14.5 kg mol^{-1}, respectively and the polydispersity index was 1.15. The volume fraction of
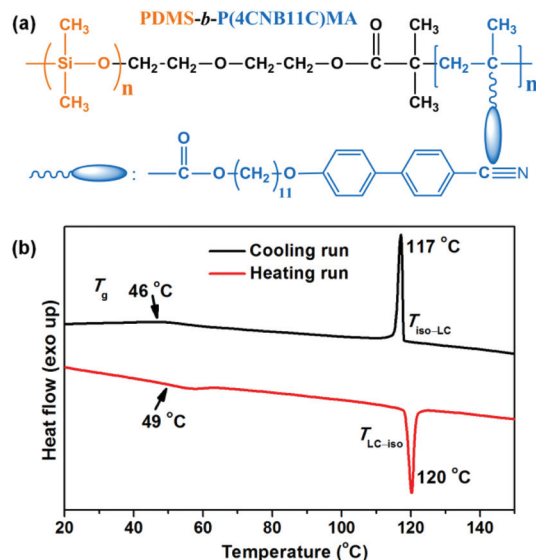

Fig. 1 (a) The chemical structure of the PDMS-*b*-P(4CNB11C)MA side chain LC block copolymer, and (b) the DSC curves of this BCP in the second heating scan (red) and in the second cooling scan (black) with a scanning rate of 5 °C min^{-1}.

PDMS was calculated to be 27% according to the molecular weights and the densities of PDMS (0.97 g cm^{-3}) and P(4CNB11C)MA (1.06 g cm^{-3}).

For the bulk samples for SAXS and TEM experiments, the block copolymer powder was dissolved in toluene solution (5.0 wt%) under overnight stirring, and the solvent was evaporated at room temperature for several days. The samples were then thermally annealed in a vacuum oven (20 Torr) for 48 h at various temperatures to induce microphase separation.

For thin film preparation, a solution of PDMS-*b*-P(4CNB11C)MA with a concentration of 5.0 wt% in toluene was made. Films with a thickness of 140 nm were spin-coated on the as-received Si substrates. The film thickness was determined by a reflectometry system (FilMetrics F20-UV) by measuring the reflectance spectra within a wavelength range of 300–1000 nm. The films were thermally annealed at different temperatures under vacuum (20 Torr) for 72 h at each temperature. Due to the lower surface energy of the PDMS block, thin wetting layers of PDMS were expected to form at the substrate surface/film interface and the film/air interface.

Thermal behavior and LC phase transition temperatures of the block copolymer were characterized using a TA Q2000 DSC (TA Instruments, USA) at heating and cooling rates of 10 °C min^{-1} under a nitrogen flow. The characteristic temperatures of the polymer were recorded from the second heating run curve and the second cooling run curve.

To identify the microphase-separated nanostructures of the block copolymer in bulk, 1D SAXS measurements were carried out on a Xeuss 2.0 instrument (Xenocs) using Cu Kα radiation at a wavelength of 0.154 nm. The working voltage and current were 50 kV and 0.6 mA, respectively. The scattering profiles of SAXS were recorded with a q range from 0.042 to 2.21 nm^{-1}.

The scattering vector q is defined as $q = 4\pi/\lambda[\sin\theta]$, where the scattering angle is 2θ, and the d-spacing (d) is given by $2\pi/q$. The phase morphologies of bulk samples were observed by TEM (FEI, USA) at 200 kV. 80–100 nm thick sections for TEM characterization were ultra-microtomed from a sample embedded in epoxy resin and were collected on carbon-coated 400-mesh copper grids.

The GISAXS and GIWAXS measurements on the thin films were performed at the Complex Materials Scattering (CMS, 11-BM) beamline of the National Synchrotron Light Source II at Brookhaven National Laboratory. X-ray energy was set to 13.5 keV, and the beam size was adjusted to 200 μm horizontal by 50 μm vertical. SAXS data were collected using a pixel-array detector (Dectris Pilatus 2M) positioned 5.090 m downstream of the sample; WAXS data were collected using a fiber-coupled CCD detector (Photonic Sciences) positioned 0.231 m downstream. Conversion to q-space was performed using a standard sample (silver behenate) for calibration. We define q_z to be the vertical (film normal) direction, and q_x to be the orthogonal horizontal (in-plane) direction.

The morphologies of the BCP thin films were characterized *ex situ* by a Zeiss Merlin high resolution scanning electron microscope (SEM) at 3 kV and a Veeco metrology nanoscope V atomic force microscope (AFM) with a dimension of 3100 in the tapping mode. The thin films for the SEM and AFM characterization were first subjected to a two-step reactive ion etching (Plasma-Therm 790) composed of 50 W CF_4 plasma at 15 mTorr for 8 s to remove the PDMS wetting layer on the surface and 90 W O_2 plasma at 6 mTorr for 20 s to selectively etch the P(4CNB11C)MA matrix, leaving oxidized PDMS microdomains on the substrates.

Results and discussion

Liquid crystalline phase behavior and microphase separation behavior in bulk

The PDMS-*b*-P(4CNB11C)MA block copolymer is a side chain liquid crystalline block copolymer with a chemical structure as shown in the scheme of Fig. 1a. We first conducted DSC measurement to characterize the thermal and liquid crystalline phase behavior of the LCBCP. As shown by the DSC curve in Fig. 1b, the block copolymer underwent two transitions during the second heating run (red curve) and during the second cooling run (black curve). The baseline shifts at around 49 °C in the DSC trace in the heating cycle correspond to the glass transition (T_g) of the P(4CNB11C)MA block, and the endothermic peak at 120 °C with an enthalpy change of 3.65 J g^{-1} is attributed to the phase transition of P(4CNB11C)MA from the smectic-A LC phase to the isotropic liquid phase (T_{LC-iso}). During the cooling cycle, the reverse isotropic liquid to the smectic phase transition (T_{iso-LC}) of the P(4CNB11C)MA block occurred at 117 °C with the enthalpy change of the exothermic peak of 3.86 J g^{-1}, and the T_g peak appeared at 46 °C.

The microphase separation of the PDMS-*b*-P(4CNB11C)MA block copolymer in bulk was investigated by SAXS and TEM experiments. Firstly the bulk samples, as-cast and annealed at 115 °C, were characterized by SAXS under ambient conditions. As shown in Fig. 2a, the SAXS profile of the as-cast sample only had one scattering peak at 0.360 nm^{-1}, corresponding to a d-spacing of 17.5 nm. The SAXS profile of the sample after annealing at 115 °C had two diffraction peaks with a scattering vector ratio of 1 : $\sqrt{3}$. The peak position of the primary scattering maximum shifted to $q^* = 0.317$ nm^{-1} corresponding to a d-spacing of 19.8 nm. Hence the annealing increased the periodicity of the nanostructure, and the intensity of the primary reflection peak became stronger which indicated the formation of a better ordered nanostructure, attributed to the mobility of the LC block above the T_g. TEM was used to confirm the morphology of the bulk sample. In the TEM images, the darker features are the PDMS microdomains and the brighter ones are the P(4CNB11C)MA microdomains, due to the higher electron density of the silicon-containing block.[47] As shown in Fig. 2b, the as-cast sample presented a hexagonal (HEX) cylindrical pattern of PDMS with a periodicity of 17.5 nm. Better ordered HEX morphologies were observed in the annealed sample as indicated by the section of the hex-
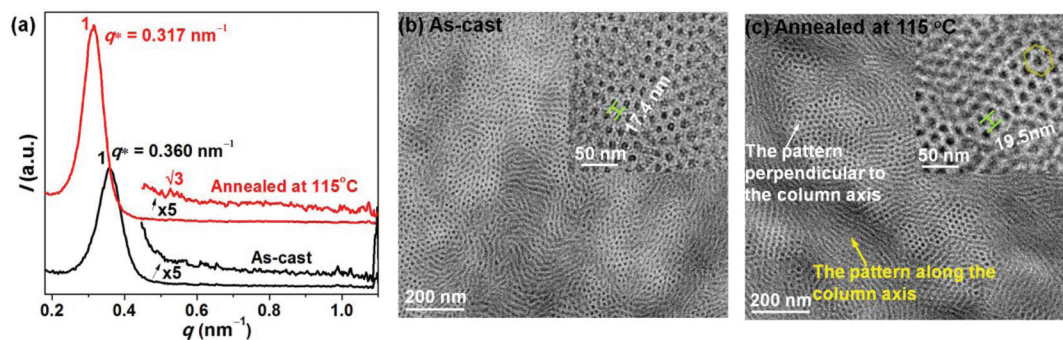
Fig. 2 (a) SAXS profiles of the PDMS-*b*-P(4CNB11C)MA as-cast (black curve) and after annealing at 115 °C (red curve); and the TEM images of the sample after drying from solution (b) and after thermal annealing at 115 °C (c) with the insets showing higher magnification images. The area indicated by the yellow arrow indicates microdomains sectioned along the hexagonal column direction and that indicated by the white arrow indicates microdomains perpendicular to the column axis of the HEX structure.
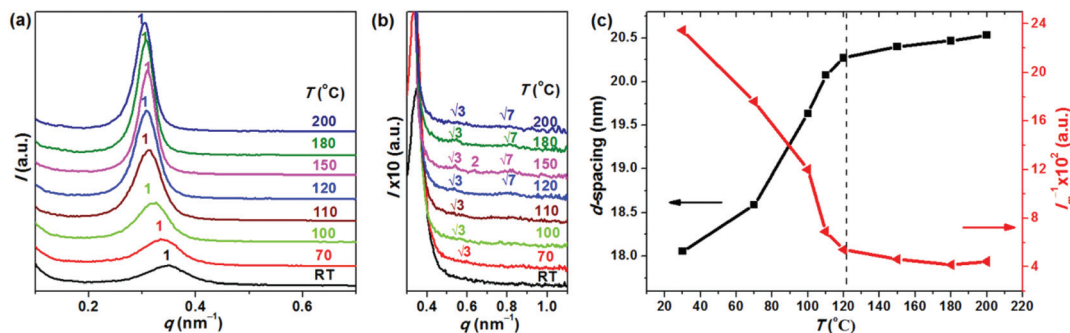
Fig. 3 (a, b) SAXS profiles measured *in situ* during the annealing of PDMS-*b*-P(4CNB11C)MA BCP. (c) The *d*-spacing values (black squares) and the reciprocal of the maximum scattering intensity of the primary scattering peak (red triangles) as a function of the temperature.

agonal packed pattern perpendicular to the column axis and the section along the column axis in Fig. 2c. As shown in the inset of Fig. 2c, the row-to-row distance of the PDMS cylinders from the TEM was about 19.5 nm, which was consistent with the values obtained from SAXS.

In situ SAXS with heating was then carried out to examine the structural transition of the PDMS-*b*-P(4CNB11C)MA block copolymer as the LC phase transformed to the isotropic state on heating. As shown in Fig. 3, the SAXS profiles of the samples measured at 70, 100, and 110 °C had two diffraction peaks with a scattering vector ratio of $1:\sqrt{3}$. The *d*-spacing and the scattering intensity of the primary scattering peak continuously increased and the half peak width decreased as the temperature increased. Measurements at 120, 150, 180 and 200 °C showed a sharper primary scattering peak and a higher reflection peak at $\sqrt{7}q^*$, and a further peak at $2q^*$ was observed at 150 °C. Therefore, the microphase-separated nanostructure remained in the HEX structure when the P(4CNB11C)MA block transformed to the isotropic phase.

The plots of the *d*-spacing value and the reciprocal of the maximum scattering intensity of the first-order diffraction (I_m^{-1}) as a function of temperature are shown in Fig. 3c. The *d*-spacing and the I_m increased quickly with temperature up to 120 °C, and then the values stabilized for higher temperatures. The *d*-spacing increase with increasing temperature up to 120 °C is attributed to chain extension which maximizes chain conformation entropy, and an increased LC ordering from the as-cast disordered chains that occurs above the glass transition temperature. Above 120 °C, the cyanobiphenyl LC groups of P(4CNB11C)MA entered the isotropic phase, but the polymer chain maintained its extended conformation and the *d*-spacing did not change much in this temperature range. The chain conformations of the block copolymer as cast, in the temperature range $T_g < T < T_{LC\text{-iso}}$ and above $T_{LC\text{-iso}}$ are illustrated in Fig. S1.† Despite the LC phase transition, the microphase separated nanostructures remained HEX for temperatures up to 200 °C according to the scattering vector ratios. We conclude that the bulk BCP self-assembled into a hierarchical nanostructure of HEX with PDMS cylinders inside a matrix of smectic P(4CNB11C)MA, and transformed to a HEX structure within isotropic P(4CNB11C)MA above 120 °C.

Self-assembly and morphology transition in thin films

Films of PDMS-*b*-P(4CNB11C)MA with a thickness of 140 nm were prepared on silicon wafers. We first describe the hierarchical nanostructure of the BCP thin film after annealing at 120 °C for 72 h. As seen in Fig. 4a, the 2D GISAXS profile showed an in-plane HEX structure, though the weak circular scattering ring indicates the coexistence of other orientations. The SEM image of Fig. 4b confirmed the in-plane cylindrical
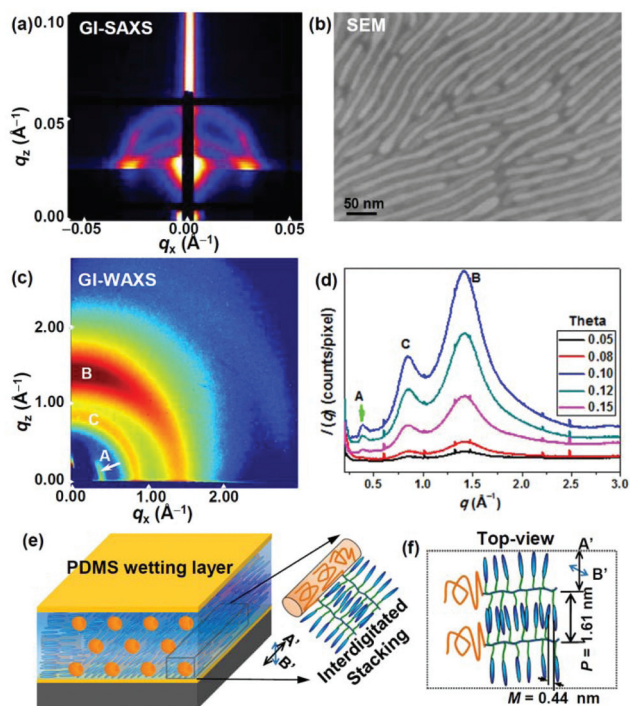
Fig. 4 (a) 2D GISAXS pattern with an incident angle of 0.15° of the 140 nm thick BCP film after annealing at 120 °C; (b) a representative SEM image of oxidized PDMS cylindrical nanopatterns formed in the thin film; (c) 2D GIWAXS pattern with an incident angle of 0.15°, and (d) the 1D GIWAXS profiles with an incident angle from 0.05° to 0.15°. (e, f) Schematic illustrations of the in-plane cylinder with LC mesogens in a smectic LC phase, where the mesogen π–π interaction direction is perpendicular to the smectic layer direction.

morphology in which the oxidized PDMS cylinders in adjacent layers were parallel to each other. The layers can be identified by their different contrast, with the top layer appearing brighter.[48] The cross-section SEM images in Fig. S2† present a closepacked arrangement of bright spots corresponding to the cross-sections of the PDMS cylinders, which also confirmed the in-plane cylindrical morphology. In the 2D GIWAXS profile (Fig. 4c), the scattering arc labelled A in the equatorial direction suggests a smectic-A LC phase of P(4CNB11C)MA, and this layered structure stacks perpendicular to the film plane. 1D GIWAXS profiles with different incident angles are plotted in Fig. 4d, and show three sets of scattering peaks. From the location of the reflection A at $q_x = 0.39$ Å^{-1}, the smectic layer spacing was determined to be 1.61 nm. From the chemical structure, the length of the LC group on the side chain was calculated as about 0.97 nm (as described in Fig. S3†) and there was a coil spacer of $-(CH_2)_{11}$ between the conjugated LC and the backbone. Therefore, the cyanobiphenyl LC groups between the neighboring chains are believed to interdigitate. The intense scattering arc B located at $q_z = 1.43$ Å^{-1}, corresponding to a d-spacing of 0.44 nm, is attributed to the interaction between the cyanobiphenyl LC mesogens of the P(4CNB11C)MA block. This result is consistent with the tendency of the cyanobiphenyl mesogens to aggregate through π–π stacking interactions. The face-to-face interaction direction of the LC mesogen should be parallel to the film plane. The other broad isotropic scattering peak C at $q_x = 0.85$ Å^{-1}, corresponding to a d-spacing of 0.74 nm, is attributed to the amorphous PDMS block.

The in-plane cylindrical structure with interdigitated stacking of the LC mesogens in a continuous smectic phase is schematically illustrated in Fig. 4e and f. The long axis of the mesogens is along the axis of the microphase separated cylinders. From the top view, the LC mesogens stacked face-to-face into a smectic phase with its molecular plane parallel to the substrate surface, and the smectic layers normal to the substrate. The periodicity of the smectic structure (P) was 1.61 nm and the mesogen to mesogen distance (M) was 0.44 nm obtained

from the GIWAXS. The smectic layering direction (noted by the double-headed black arrows A′) is normal to the mesogen face-to-face interaction direction indicated by the double-headed blue arrows B′ (Fig. 4f). Therefore, the hierarchical structure consists of three levels of ordering: the mesogen orientation, the smectic LC orientation and the orientation of the microphase-separated domains. Furthermore, the drop-cast thick film of this BCP annealed at 120 °C also presented good in-plane ordering of the cylindrical nanostructure as shown in Fig. S4.†

We now describe the structural evolution of the block copolymer films during thermal annealing using *in situ* GISAXS and GIWAXS. 2D GISAXS and GIWAXS profiles with the same incident angle of 0.15° during the thermal annealing process after holding for 10 min at each temperature are compared in Fig. 5(a–f) and (g–l).

For the as-cast film at 30 °C, the GISAXS profile exhibited a broad scattering ring, indicative of a poorly-ordered microphase-separated structure kinetically trapped during spin-coating from solution, while the LC block was in the smectic A phase based on the arc A in the equatorial direction at $q = 0.39$ Å^{-1}. When the temperature increased to 50 °C, intense scattering rings appeared in the GISAXS profile, suggesting the emergence of poorly oriented hexagonally packed cylinders. The LC block was in a more ordered smectic phase (indicated by the sharper scattering intensity at A and B in the GIWAXS profile) due to the mobility of the backbone of the LC block near the T_g of P(4CNB11C)MA. When the temperature increased to 120 °C, the intensity of the GISAXS increased and scattering peaks appeared while the rings became faint, indicative of the increased in-plane ordering of the cylindrical morphology. The scattering peaks at A and B of the GIWAXS profile became broad indicating the LC block becoming disordered as the temperature approached the smectic-to-isotropic transition temperature.

When the temperature increased above 140 °C, the GISAXS and GIWAXS underwent drastic changes. At 140 °C, the
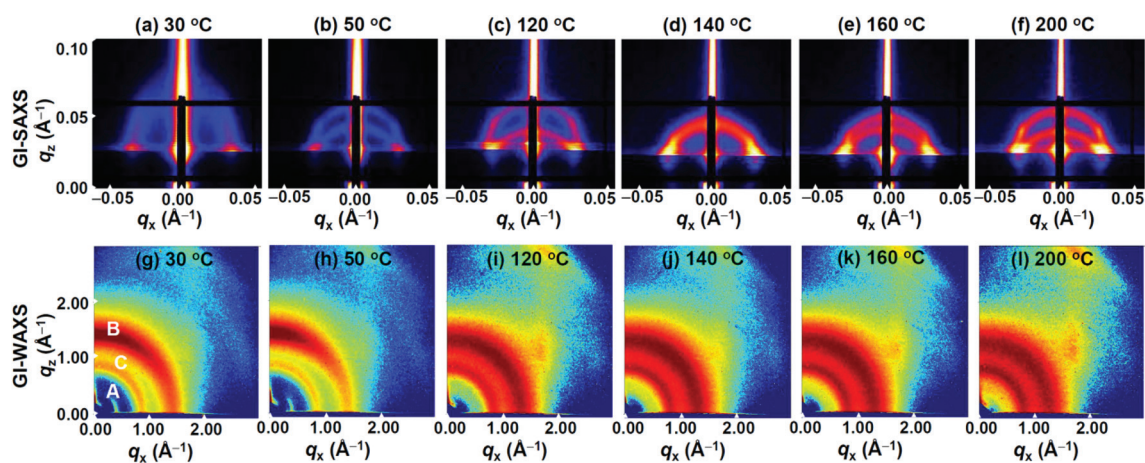

Fig. 5 *In situ* GISAXS 2D patterns (a–f) and *in situ* GIWAXS 2D patterns (g–l) of the PDMS-*b*-P(4CNB11C)MA BCP thin film at the indicated temperatures during thermal annealing.

GISAXS profile became a merged halo. The position of the first q_x scattering peak did not change, but the position of the ring at q_z decreased, which is attributed to structural undulations as P(4CNB11C)MA transformed to the isotropic phase. When the temperature increased to 160 °C, the two rings and scattering peaks appeared again, and the scattering intensity increased further at 200 °C, but the q_x value of the first scattering peak showed little change. The GIWAXS profiles above 140 °C showed a featureless pattern except for two isotropic amorphous rings corresponding to the isotropic PDMS (centered at $q_x = 0.85$ Å^{-1}) and isotropic P(4CNB11C)MA (centered at $q_x = 1.42$ Å^{-1}). As the temperature increased, the isotropic amorphous ring of P(4CNB11C)MA became broader and more ambiguous, as a result of the increased undulation of the backbone of P(4CNB11C)MA. The GIWAXS and GISAXS results collectively indicated that the microphase-separated nanostructure experienced an order-to-order transition as the P(4CNB11C)MA block transformed from the smectic LC phase to the isotropic phase.

SEM and AFM experiments were carried out on thin films annealed in air at different temperatures and then quenched to room temperature. Representative SEM images of the films after etching are shown in Fig. S5† and Fig. 6, in which P(4CNB11C)MA has been etched and the oxidized PDMS patterns were revealed, appearing bright.

The morphology of the thin film without thermal annealing was a mixture of disordered spheres and short cylinder segments as shown in Fig. S5,† consistent with the GISAXS result. After quenching from 120 °C (Fig. 6(a and b)), an in-plane HEX morphology was observed with parallel cylinders in the upper and lower layers indicated by the white and yellow arrows. The cylinder-to-cylinder distance in the SEM image is about 22.2 nm which is close to the center-to-center distance $(2d/\sqrt{3}, \sim22.8$ nm) of the cylinders in the bulk sample. In films on a bare silicon wafer, the PDMS wetting layers at the film/substrate interface and the film/air surface result in symmetrical wetting, so that the commensurate film thickness is nd (d is the layer spacing of the HEX structure). The film thickness (140 nm) is close to $7d$, where d is 19.7 nm, and the cross-section SEM image shown in Fig. 2 presented 7 layers of cylinders.

SEM images of the thin film quenched from 160 °C show the coexistence of PDMS spheres, ellipsoids and short cylinders, Fig. 6(c and d). From their relative orientation, it appears that they represent a partial conversion of the HEX cylinders to a BCC symmetry. After quenching from 200 °C, only a PDMS spherical morphology was observed in Fig. 6(e and f). Therefore, the HEX to BCC structure transition of the microphase-separated nanostructure appeared between 160 °C and 200 °C. Fig. 6(c and d) represent a transient state between HEX and BCC.

The HEX to BCC transition as well as the transient morphology of the thin film was further confirmed by AFM experiments. The AFM height and phase images of the etched thin films after annealing at 120, 160 and 200 °C are compared in Fig. 7, and the morphologies were consistent with the SEM results.

From the morphology of the transient state, the spheres formed from the cylinders had six-fold symmetry as noted by the green hexagon in Fig. 6d, which indicates that the decomposition of the cylinder into spheres should be along the (111) direction of the BCC structure. The structure models
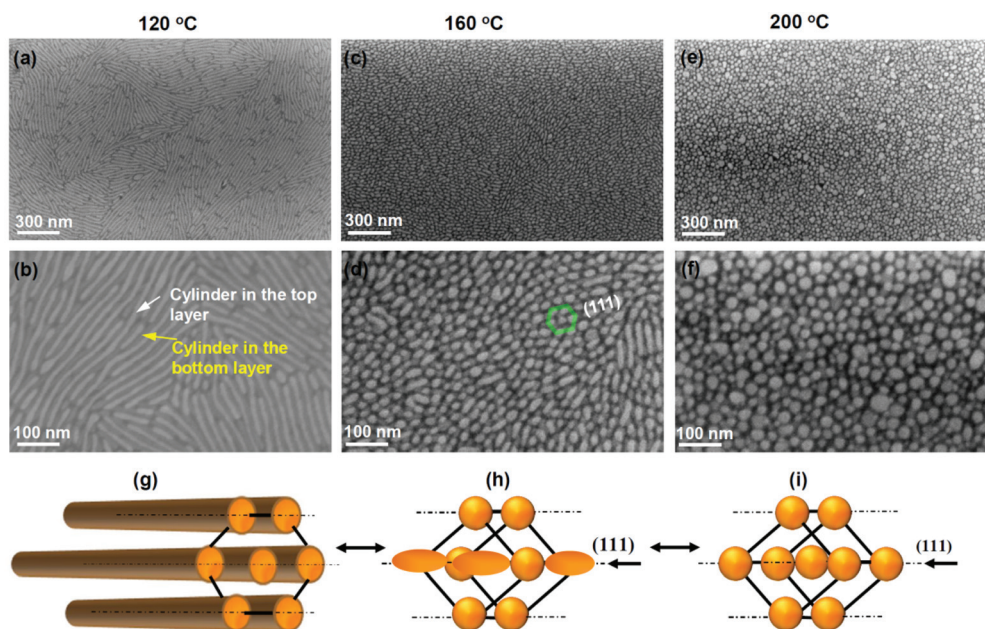

Fig. 6 SEM images of oxidized PDMS patterns from the thin films of PDMS-*b*-P(4CNB11C)MA BCP quenched from (a, b) 120 °C, (c, d) 160 °C and (e, f) 200 °C, and (g−i) a schematic illustration of the HEX to BCC transition.
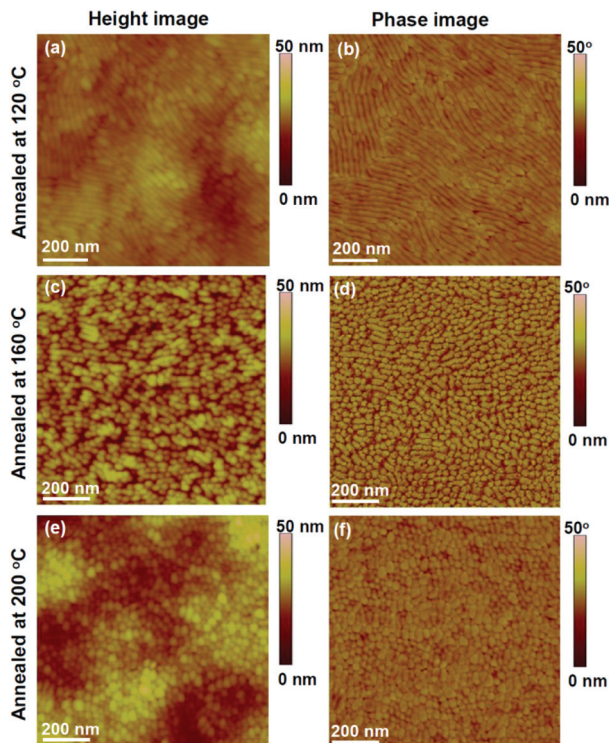
Fig. 7 AFM height images (left) and phase images (right) of the PDMS-*b*-P(4CNB11C)MA BCP thin films on silicon substrates after quenching from (a, b) 120 °C, (c, d) 160 °C and (e, f) 200 °C.

and the transition process are schematically illustrated in Fig. 6(g–i). From the suggested transition pathway, we expect that the (110) *d*-spacing of the BCC sphere lattice should equal the (100) *d*-spacing of the hexagonal cylinder lattice. This can explain the fact that the q_x value of the first scattering peak of the BCC in the GISAXS profile at 200 °C was almost the same as that of the HEX structure at 120 °C. The nearest neighbor (NN) spacing of the BCC structures obtained from the GISAXS should be d_{110}, which matched the NN spacing of the hexagonal cylinders from the GISAXS, d_{100}.[49,50] This study therefore identifies the pathway of the HEX to BCC transition from the transient morphology observed by SEM and AFM.

Several factors influence the HEX to BCC structural transition including the LC phase transition, variation of the Flory–Huggins interaction parameter (χ), and the composition of the block copolymer. The PDMS-containing liquid crystalline block copolymer is expected to have an intrinsically high interaction parameter χ, and below 120 °C, the smectic LC phase of the P(4CNB11C)MA block makes a positive contribution, χ_{LC}, to the effective interaction parameter, χ_{eff}.[51] The volume fraction of the LC block is $f_{P(4CNB11C)MA}$ ~73% and the $\chi_{eff}N$ falls within the HEX region in the phase diagram. Moreover, the smectic LC ordering favors a cylindrical morphology compared to spherical due to the interfacial curvature. After the P(4CNB11C)MA block transformed from the smectic LC phase to an isotropic phase above 120 °C, and the influence of the LC ordering on the microphase separation dis-

appeared, the χ_{eff} decreased. However, the microphase separated nanostructure was still cylindrical in the temperature range from 120 to 140 °C. The χ_{eff} continued to decrease with increasing temperature, since $\chi(T)$ scales inversely with temperature, and we conclude that the morphology enters the BCC regime in the phase diagram at ~160 °C. A transient morphology from HEX to BCC was observed in the thin film quenched from 160 °C, which is higher than the temperature of 140 °C for the structural transition observed in GISAXS. This may be a result of a reverse transition of the sample during cooling: the BCC structure in the sample used for SEM imaging had partly converted back to HEX on cooling. The evolution of $\chi_{eff}N$ is indicated schematically in the phase diagram in Fig. S6.† The lack of the HEX-BCC transformation in the bulk sample is a contrast to the thin film results. Differences in the morphology between films and bulk may be caused by surface energy effects or by the geometrical constraint caused by the film thickness, but the origin of this difference in the LC BCP requires further investigation.

Conclusions

In summary, the bulk and thin film self-assembly of a silicon-containing side-chain liquid crystalline block copolymer PDMS-*b*-P(4CNB11C)MA was investigated. In bulk, the PDMS-*b*-P(4CNB11C)MA block copolymer with f_{PDMS} 27% formed a hierarchical nanostructure of PDMS cylinders within a LC P(4CNB11C)MA matrix, which transformed from a smectic to an isotropic LC phase on heating above 120 °C. Thin films of this block copolymer also presented a cylindrical morphology with in-plane oriented PDMS cylinders. The mesogen orientation and the smectic LC orientation were related to the microdomain orientation, thus the thin film morphology constrains these orientations compared to the bulk. The *in situ* GISAXS and GIWAXS and *ex situ* AFM and SEM measurements revealed a HEX to BCC structural transition of the thin film at ~160 °C that was not seen in the bulk BCP up to 200 °C. The hierarchical ordering of the microdomains and mesogens, as well as the high-χ value and the etch contrast in an oxygen plasma, makes this silicon-containing LC block copolymer an attractive system for nanoscale fabrication.

Conflicts of interest

There are no conflicts to declare.

Acknowledgements

Notes and references

1 F. S. Bates and G. H. Fredrickson, Block Copolymers—Designer Soft Materials, *Phys. Today*, 1999, **52**, 32–38.

2 S. Valkama, H. Kosonen, J. Ruokolainen, T. Haatainen, M. Torkkeli, R. Serimaa, G. Ten Brinke and O. Ikkala, Self-assembled polymeric solid films with temperature-induced large and reversible photonic-bandgap switching, *Nat. Mater.*, 2004, **3**, 872–876.

3 H. S. Suh, D. H. Kim, P. Moni, S. Xiong, L. E. Ocola, N. J. Zaluzec, K. K. Gleason and P. F. Nealey, Sub-10 nm patterning via directed self-assembly of block copolymer films with a vapour-phase deposited topcoat, *Nat. Nanotechnol.*, 2017, **12**, 575.

4 C. M. Bates and F. S. Bates, 50th Anniversary Perspective: Block Polymers—Pure Potential, *Macromolecules*, 2017, **50**, 3–22.

5 H. Ahn, S. Park, S.-W. Kim, P. J. Yoo, D. Y. Ryu and T. P. Russell, Nanoporous Block Copolymer Membranes for Ultrafiltration: A Simple Approach to Size Tunability, *ACS Nano*, 2014, **8**, 11745–11752.

6 R. Deng, F. Liang, P. Zhou, C. Zhang, X. Qu, Q. Wang, J. Li, J. Zhu and Z. Yang, Janus Nanodisc of Diblock Copolymers, *Adv. Mater.*, 2014, **26**, 4469–4472.

7 C. M. Bates, T. Seshimo, M. J. Maher, W. J. Durand, J. D. Cushen, L. M. Dean, G. Blachut, C. J. Ellison and C. G. Willson, Polarity-Switching Top Coats Enable Orientation of Sub-10 nm Block Copolymer Domains, *Science*, 2012, **338**, 775.

8 S. Lee, L.-C. Cheng, K. R. Gadelrab, K. Ntetsikas, D. Moschovas, K. G. Yager, A. Avgeropoulos, A. Alexander-Katz and C. A. Ross, Double-Layer Morphologies from a Silicon-Containing ABA Triblock Copolymer, *ACS Nano*, 2018, **12**, 6193–6202.

9 T. Kato, N. Mizoshita and K. Kishimoto, Functional Liquid-Crystalline Assemblies: Self-Organized Soft Materials, *Angew. Chem., Int. Ed.*, 2005, **45**, 38–68.

10 C. Tschierske, Liquid crystal engineering – new complex mesophase structures and their relations to polymer morphologies, nanoscale patterning and crystal engineering, *Chem. Soc. Rev.*, 2007, **36**, 1930–1970.

11 K. Mukai, M. Hara, S. Nagano and T. Seki, High-Density Liquid-Crystalline Polymer Brushes Formed by Surface Segregation and Self-Assembly, *Angew. Chem., Int. Ed.*, 2016, **55**, 14028–14032.

12 J. Kao, K. Thorkelsson, P. Bai, B. J. Rancatore and T. Xu, Toward functional nanocomposites: taking the best of nanoparticles, polymers, and small molecules, *Chem. Soc. Rev.*, 2013, **42**, 2654–2678.

13 T. M. S. K. Pathiranage, M. Kim, H. Q. Nguyen, K. E. Washington, M. C. Biewer and M. C. Stefan, Enhancing Long-Range Ordering of P3HT by Incorporating Thermotropic Biphenyl Mesogens via ATRP, *Macromolecules*, 2016, **49**, 6846–6857.

14 I. W. Hamley, V. Castelletto, Z. B. Lu, C. T. Imrie, T. Itoh and M. Al-Hussein, Interplay between Smectic Ordering and Microphase Separation in a Series of Side-Group Liquid-Crystal Block Copolymers, *Macromolecules*, 2004, **37**, 4798–4807.

15 H. Yu, Photoresponsive liquid crystalline block copolymers: From photonics to nanotechnology, *Prog. Polym. Sci.*, 2014, **39**, 781–815.

16 J. Sänger, W. Gronski, S. Maas, B. Stühn and B. Heck, Structural Transition in a Nematic LC Block Copolymer Induced by the Transition to the LC Phase, *Macromolecules*, 1997, **30**, 6783–6787.

17 M. Muthukumar, C. K. Ober and E. L. Thomas, Competing Interactions and Levels of Ordering in Self-Organizing Polymeric Materials, *Science*, 1997, **277**, 1225–1232.

18 M. Gopinadhan, Y. Choo and C. O. Osuji, Strong Orientational Coupling of Block Copolymer Microdomains to Smectic Layering Revealed by Magnetic Field Alignment, *ACS Macro Lett.*, 2016, **5**, 292–296.

19 M. Sano, M. Hara, S. Nagano, Y. Shinohara, Y. Amemiya and T. Seki, New Aspects for the Hierarchical Cooperative Motions in Photoalignment Process of Liquid Crystalline Block Copolymer Films, *Macromolecules*, 2015, **48**, 2217–2223.

20 E. Verploegen, T. Zhang, Y. S. Jung, C. Ross and P. T. Hammond, Controlling the Morphology of Side Chain Liquid Crystalline Block Copolymer Thin Films through Variations in Liquid Crystalline Content, *Nano Lett.*, 2008, **8**, 3434–3440.

21 P. Deshmukh, S.-k. Ahn, L. Geelhand de Merxem and R. M. Kasi, Interplay between Liquid Crystalline Order and Microphase Segregation on the Self-Assembly of Side-Chain Liquid Crystalline Brush Block Copolymers, *Macromolecules*, 2013, **46**, 8245–8252.

22 K. Nickmans, J. N. Murphy, B. de Waal, P. Leclère, J. Doise, R. Gronheid, D. J. Broer and A. P. H. J. Schenning, Sub-5 nm Patterning by Directed Self-Assembly of Oligo (Dimethylsiloxane) Liquid Crystal Thin Films, *Adv. Mater.*, 2016, **28**, 10068–10072.

23 C. Sinturel, F. S. Bates and M. A. Hillmyer, High χ–Low N Block Polymers: How Far Can We Go?, *ACS Macro Lett.*, 2015, **4**, 1044–1050.

24 M. Huang, K. Yue, J. Huang, C. Liu, Z. Zhou, J. Wang, K. Wu, W. Shan, A.-C. Shi and S. Z. D. Cheng, Highly Asymmetric Phase Behaviors of Polyhedral Oligomeric Silsesquioxane-Based Multiheaded Giant Surfactants, *ACS Nano*, 2018, **12**, 1868–1877.

25 T.-Y. Lo, M. R. Krishnan, K.-Y. Lu and R.-M. Ho, Silicon-containing block copolymers for lithographic applications, *Prog. Polym. Sci.*, 2018, **77**, 19–68.

26 K. Aissou, M. Mumtaz, G. Fleury, G. Portale, C. Navarro, E. Cloutet, C. Brochon, C. A. Ross and G. Hadziioannou, Sub-10 nm Features Obtained from Directed Self-Assembly of Semicrystalline Polycarbosilane-Based Block Copolymer Thin Films, *Adv. Mater.*, 2015, **27**, 261–265.

27 V. P. Chuang, C. A. Ross, J. Gwyther and I. Manners, Self-Assembled Nanoscale Ring Arrays from a Polystyrene-b-polyferrocenylsilane-b-poly(2-vinylpyridine)Triblock Terpolymer Thin Film, *Adv. Mater.*, 2009, **21**, 3789–3793.

28 Y. S. Jung and C. A. Ross, Orientation-Controlled Self-Assembled Nanolithography Using a Polystyrene−Polydimethylsiloxane Block Copolymer, *Nano Lett.*, 2007, **7**, 2046–2050.

29 T. Kun-Hua, B. Wubin, L. George, N. Konstantinos, A. Apostolos and A. R. Caroline, Universal pattern transfer methods for metal nanostructures by block copolymer lithography, *Nanotechnology*, 2015, **26**, 375301.

30 W. Li and M. Müller, Directed self-assembly of block copolymers by chemical or topographical guiding patterns: Optimizing molecular architecture, thin-film properties, and kinetics, *Prog. Polym. Sci.*, 2016, **54–55**, 47–75.

31 T. P. Russell and Y. Chai, 50th Anniversary Perspective: Putting the Squeeze on Polymers: A Perspective on Polymer Thin Films and Interfaces, *Macromolecules*, 2017, **50**, 4597–4609.

32 S. Ji, L. Wan, C.-C. Liu and P. F. Nealey, Directed self-assembly of block copolymers on chemical patterns: A platform for nanofabrication, *Prog. Polym. Sci.*, 2016, **54–55**, 76–127.

33 K. Fukuhara, S. Nagano, M. Hara and T. Seki, Free-surface molecular command systems for photoalignment of liquid crystalline materials, *Nat. Commun.*, 2014, **5**, 3320.

34 Y. Morikawa, S. Nagano, K. Watanabe, K. Kamata, T. Iyoda and T. Seki, Optical Alignment and Patterning of Nanoscale Microdomains in a Block Copolymer Thin Film, *Adv. Mater.*, 2006, **18**, 883–886.

35 T. Wang, X. Li, Z. Dong, S. Huang and H. Yu, Vertical Orientation of Nanocylinders in Liquid-Crystalline Block Copolymers Directed by Light, *ACS Appl. Mater. Interfaces*, 2017, **9**, 24864–24872.

36 H.-L. Xie, X. Li, J. Ren, C. Bishop, G. Arges Christopher and F. Nealey Paul, Controlling domain orientation of liquid crystalline block copolymer in thin films through tuning mesogenic chemical structures, *J. Polym. Sci., Part B: Polym. Phys.*, 2017, **55**, 532–541.

37 L. H. Mahajan, D. Ndaya, P. Deshmukh, X. Peng, M. Gopinadhan, C. O. Osuji and R. M. Kasi, Optically Active Elastomers from Liquid Crystalline Comb Copolymers with Dual Physical and Chemical Cross-Links, *Macromolecules*, 2017, **50**, 5929–5939.

38 M. Gopinadhan, Y. Choo, K. Kawabata, G. Kaufman, X. Feng, X. Di, Y. Rokhlenko, L. H. Mahajan, D. Ndaya, R. M. Kasi and C. O. Osuji, Controlling orientational order

in block copolymers using low-intensity magnetic fields, *Proc. Natl. Acad. Sci. U. S. A.*, 2017, **114**, E9437–E9444.

39 K. Nickmans, M. Bögels Gerardus, C. Sánchez-Somolinos, N. Murphy Jeffrey, P. Leclère, K. Voets Ilja and P. H. J. Schenning Albertus, 3D Orientational Control in Self-Assembled Thin Films with Sub-5 nm Features by Light, *Small*, 2017, **13**, 1701043.

40 J. Raybin, J. Ren, X. Chen, R. Gronheid, P. F. Nealey and S. J. Sibener, Real-Time Atomic Force Microscopy Imaging of Block Copolymer Directed Self Assembly, *Nano Lett.*, 2017, **17**, 7717–7723.

41 Y. Choo, P. W. Majewski, M. Fukuto, C. O. Osuji and K. G. Yager, Pathway-engineering for highly-aligned block copolymer arrays, *Nanoscale*, 2018, **10**, 416–427.

42 P. W. Majewski and K. G. Yager, Reordering transitions during annealing of block copolymer cylinder phases, *Soft Matter*, 2016, **12**, 281–294.

43 C. T. Black, C. Forrey and K. G. Yager, Thickness-dependence of block copolymer coarsening kinetics, *Soft Matter*, 2017, **13**, 3275–3283.

44 M. Komura, H. Komiyama, K. Nagai and T. Iyoda, Direct Observation of Faceted Grain Growth of Hexagonal Cylinder Domains in a Side Chain Liquid Crystalline Block Copolymer Matrix, *Macromolecules*, 2013, **46**, 9013–9020.

45 H. Komiyama, R. Sakai, S. Hadano, S. Asaoka, K. Kamata, T. Iyoda, M. Komura, T. Yamada and H. Yoshida, Enormously Wide Range Cylinder Phase of Liquid Crystalline PEO-b-PMA(Az) Block Copolymer, *Macromolecules*, 2014, **47**, 1777–1782.

46 S. Fu and Y. Zhao, Orientation of Azobenzene Mesogens in Side-Chain Liquid Crystalline Polymers: Interplay between Effects of Mechanical Stretching, Photoisomerization and Thermal Annealing, *Macromolecules*, 2015, **48**, 5088–5098.

47 G. H. Michler, in *Electron Microscopy of Polymers*, Springer-Verlag, Berlin, 2008.

48 W. Bai, A. F. Hannon, K. W. Gotrik, H. K. Choi, K. Aissou, G. Liontos, K. Ntetsikas, A. Alexander-Katz, A. Avgeropoulos and C. A. Ross, Thin Film Morphologies of Bulk-Gyroid Polystyrene-block-polydimethylsiloxane under Solvent Vapor Annealing, *Macromolecules*, 2014, **47**, 6000–6008.

49 L.-Y. Shi, I. F. Hsieh, Y. Zhou, X. Yu, H.-J. Tian, Y. Pan, X.-H. Fan and Z. Shen, Thermoreversible Order–Order Transition of a Diblock Copolymer Induced by the Unusual Coil–Rod Conformational Change of One Block, *Macromolecules*, 2012, **45**, 9719–9726.

50 M. Y. Paik, J. K. Bosworth, D.-M. Smilges, E. L. Schwartz, X. Andre and C. K. Ober, Reversible Morphology Control in Block Copolymer Films via Solvent Vapor Processing: An in Situ GISAXS Study, *Macromolecules*, 2010, **43**, 4253–4260.

51 W. Y. Zheng and P. T. Hammond, Phase Behavior of New Side Chain Smectic C* Liquid Crystalline Block Copolymers, *Macromolecules*, 1998, **31**, 711–721.